Available online at www.sciencedirect.com
ScienceDirect
C. R. Physique 10 (2009) 894–906
COMPTES RENDUS PHYSIQUE

Experimental determination of Boltzmann's constant

On the determination of the Boltzmann constant by means of precision molecular spectroscopy in the near-infrared

Antonio Castrillo [a], Giovanni Casa [a], Andrea Merlone [b], Gianluca Galzerano [c], Paolo Laporta [c], Livio Gianfrani [a,*]

[a] *Dipartimento di Scienze Ambientali, Seconda Università di Napoli, and CNISM – Unità Napoli 2, Via Vivaldi 43, 81100 Caserta, Italy*
[b] *Istituto Nazionale di Ricerca Metrologica, Torino, Italy*
[c] *Dipartimento di Fisica, Politecnico di Milano and Istituto di Fotonica e Nanotecnologie (IFN-CNR), Milano, Italy*

Abstract

Intensity-stabilized laser absorption spectroscopy, in the near-infrared, represents an extremely powerful tool for primary gas thermometry, provided that an accurate procedure of frequency calibration is used. The method consists in retrieving the Doppler width from highly accurate observations of the shape of a spectral line in any atomic or molecular system in the gas phase, at the thermodynamic equilibrium. Applied to CO_2 samples in the 2-μm wavelength region, it has recently allowed to perform a spectroscopic determination of the Boltzmann constant with a relative accuracy of 1.6×10^{-4}. We here discuss the main factors, of both fundamental and technical nature, limiting the accuracy of this method and report on the possibility of approaching the target accuracy of 10^{-6} by changing the molecular sample, the operation wavelength and the frequency calibration technique. ***To cite this article: A. Castrillo et al., C. R. Physique 10 (2009).***

Résumé

Vers une détermination de la constante de Boltzmann par spectroscopie laser moléculaire dans l'infrarouge proche. La spectroscopie d'absorption laser, dans le domaine de l'infrarouge proche, s'avère une puissante méthode pour la thermométrie primaire à gaz. L'objectif expérimental est de déterminer la largeur Doppler à partir d'une analyse très précise de la forme des raies d'absorption linéaire observées dans un système atomique ou moléculaire en phase gazeuse à l'équilibre thermodynamique. Appliquée au gaz carbonique à la longueur d'onde de 2-μm, cette technique a permis de déterminer la constante de Boltzmann avec une exactitude relative de 1.6×10^{-4}. Cet article analyse les facteurs principaux, de nature fondamentale ou instrumentale, qui peuvent limiter l'exactitude obtenue. Il suggère également que, en changeant la nature du gaz, la longueur d'onde du laser et la méthode d'étalonnage en fréquence, une exactitude meilleure que 10^{-6} en valeur relative peut être atteinte. ***Pour citer cet article : A. Castrillo et al., C. R. Physique 10 (2009).***

Keywords: Laser spectroscopy; Spectral line shapes; Determination of fundamental constants

Mots-clés : Spectroscopie laser ; Forme de raie ; Constantes fondamentales

* Corresponding author.
E-mail address: livio.gianfrani@unina2.it (L. Gianfrani).

1631-0705/$ – see front matter
doi:10.1016/j.crhy.2009.10.010

1. Introduction

The spectral line shape of atomic and molecular resonances, when recorded very precisely in a linear regime of interaction at the Doppler-limited resolution, for an absorbing medium in the gas phase at thermodynamic equilibrium, provides a variety of detailed physical information on the gas itself, from the macroscopic point of view, as well as on the individual particles. In fact, from the accurate analysis of an absorption profile, it is possible to retrieve, through the Beer–Lambert's law, the strength of a given line, from which the transition dipole moment between two quantum states can be inferred. Similarly, if the line strength is known, the molecular absorber density can be accurately determined. In reason of that, laser absorption spectroscopy has been recently proposed as a primary method, in alternative to gravimetry, for measuring the amount of substance in the gas phase [1].

Spectral line shapes are influenced by two main factors: collisions between the molecules and the random thermal motion of the absorbing particles. A first order representation of the these spectral broadening effects is given by the Voigt function, which is the convolution of Lorentzian and Gaussian profiles. The width of the Gaussian component is usually referred to as the Doppler width (HWHM) of the spectral line, which is given by:

$$\Delta\nu_D = \frac{\nu_0}{c}\sqrt{2\ln 2 k_B \frac{T}{m}} \tag{1}$$

where m is the mass of the molecule, T the absolute temperature, ν_0 the line center frequency, and k_B the Boltzmann constant. The equation above makes it possible to use laser absorption spectroscopy as a primary thermometric method, with the advantage of being conceptually simple, applicable to any gas at any temperature, in whatever spectral region. In contrast to other thermometric methods also based on electromagnetic radiation measurements, such as total radiation thermometry, this new approach does not require absolute radiation determinations. But, is this really a new approach? It has been known for decades that laser absorption spectroscopy could provide one of the most direct tool to determine the gas temperature, but only recently a spectroscopic determination of the Boltzmann constant has been suggested, based upon Eq. (1) [2,3]. Coming back to the absolute temperature, different measurement principles have been preferred, rather than Eq. (1), being well known how hard could be the task of observing the line shape with a high experimental accuracy and retrieve the Doppler width from a line fitting procedure. Thus, in the last ten years, we have seen several implementations of the so-called "two lines ratio method". In this case, the strategy for measuring the gas temperature is based on the determination of the intensity ratio of two molecular absorption lines, which, for optimum sensitivity, has to be properly selected [4]. One of the earliest implementation of this method was based on the use of two InGaAsP distributed feedback (DFB) diode lasers, emitting at 1347 and 1392 nm, in coincidence with a pair of H_2O vibro-rotational transitions [5]. More recently, scientists from University of Toronto have reported temperature measurements with an accuracy level of 0.2% in a CO gas [6]. The main limitation of this method can be ascribed to the fact that an accurate knowledge of the line intensity ratio, at a reference temperature, is required. Continuous improvements in the accuracy of diode laser spectrometry in the near-infrared, but also the significant advances which have been achieved in theoretical reconstruction of the spectral line profiles [7], has recently stimulated our interest towards the spectroscopic determination of the gas temperature through accurate Doppler width measurements. Thus, we have reported on a new implementation of primary gas thermometry based on laser absorption spectroscopy on CO_2 gas samples, in the wavelength region around 2 μm [8]. Doppler width determinations as a function of gas temperature, ranging between the triple point of water and the gallium melting point, allowed for a spectroscopic determination of the Boltzmann constant with a relative accuracy of about 1.6×10^{-4}, namely $k_B = 1.38058\ (22) \times 10^{-23}\ \mathrm{J\,K^{-1}}$. Here, we discuss in much more detail that experiment, also focusing on the line shape problem. Moreover, we report on the possibility of improving the accuracy by changing the molecular target and by shifting the operation wavelength down to 1.4 μm. Our efforts are aimed at approaching a relative uncertainty of 10^{-6} in order to contribute to a new definition of the unit kelvin. It must be said that the first spectroscopic determination of k_B has been performed in the mid-infrared by the Paris group of Bordé and Chardonnet, on the ν_2 asQ(6; 3) rovibrational line of the ammonia molecule $^{14}NH_3$ at a frequency of 28 953 694 MHz [9], using a CO_2 laser frequency stabilized on a OsO_4 line. In comparison to the French experiment, our work differs in several respects: the laser source, the spectral region, the molecular sample, the spectra analysis procedure and the experimental strategy for retrieving k_B.

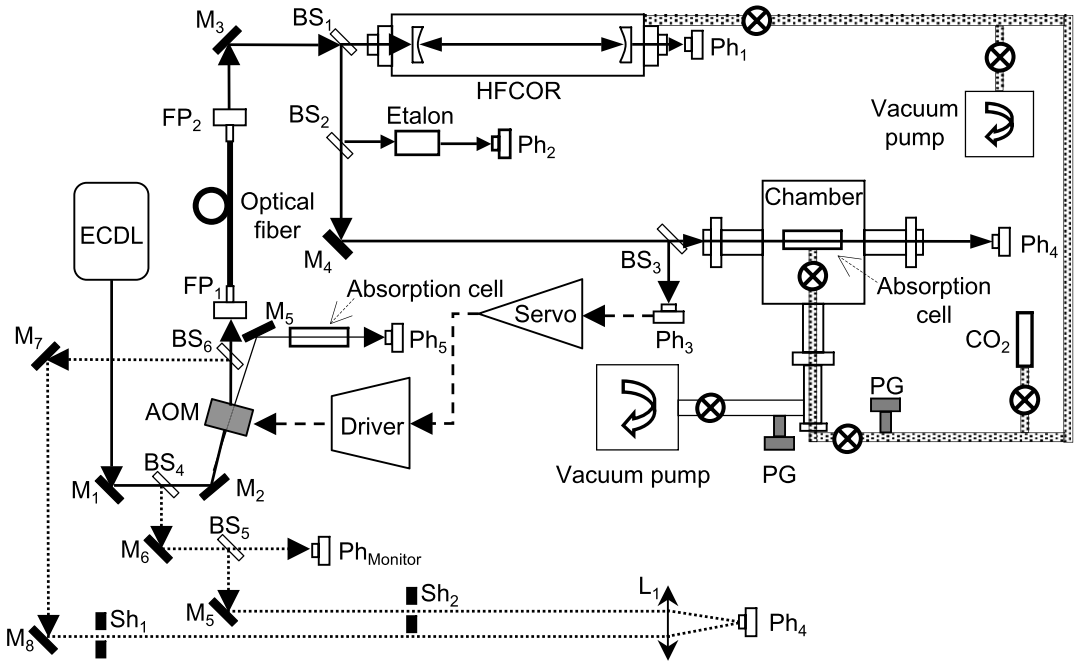

Fig. 1. A sketch of the experimental setup. ECDL: extended-cavity diode laser; HFCOR: high-finesse confocal optical resonator; M: mirror; BS: beam splitter; FP: fiber port; Ph: photodetector; PG: pressure gauge; L: lens; Sh: shutter. Beam splitters BS_4, BS_5 and BS_6 were inserted only once, at the purpose of investigating the linearity feature of Ph_4, and subsequently removed.

2. Experimental details

We perform absorption spectroscopy on a CO_2 gas sample at thermodynamic equilibrium, probing the R(12) component of the $\nu_1 + 2\nu_2^0 + \nu_3$ combination band. The experimental setup, depicted in Fig. 1, was already described in [8]. Hence, we limit this section to recalling the most important details and discussing certain aspects of the methodology that are particularly relevant for temperature determinations. A distributed feedback (DFB) diode laser, emitting on a single mode near 2.006 μm, was used as tunable laser source. It was mounted in a mirror-extended cavity configuration, with a beam splitter providing the optical feedback that narrowed the laser line width down to about 1 MHz. A homemade low-noise current supply and temperature controller was used to drive the laser and to stabilize its temperature within 1 mK. Fine and coarse wavelength tuning was done by changing the injection current (at about 1 GHz/mA) and the laser temperature (at ∼10 GHz/K), respectively. In order to scan the laser over the selected absorption line, a low frequency triangular ramp, at rate of 5 Hz, was added to the laser diode injection current, and simultaneously it was applied to a piezo-electric actuator used to change the external cavity length.

The laser's output was collimated by a double-aspheric lens and, after passing through an acousto–optic modulator (AOM), was injected into a single-mode, polarization-maintaining optical fiber used as a high-quality spatial filter to produce an optimum TEM_{00} transverse mode. The AOM, optimized for operation at 2.006 μm, was used as an actuator within a servo loop in order to keep the intensity of the laser beam constant over a laser frequency scan of half a wavenumber. Driven by a 1-W radio frequency signal at 80 MHz and properly aligned, the AOM allowed us to deflect from the primary beam to the first diffracted order about 70% of the available laser power. After the propagation inside the optical fiber and the subsequent recollimation, the laser beam was split into four different parts by a series of beam splitters. The first part was sent to a high-finesse, confocal optical resonator that provides accurate frequency markers for calibration purposes. The second beam was sent to a 5-cm thick germanium etalon, which allowed for a further coarse check of the frequency calibration. The third beam was focused into a photodiode, whose output signal was used as the input signal to a proportional-integrator circuit to actively control the RF power driving the AOM, in order to keep the 1st-order power constant. Finally, the remaining portion of the laser beam passed through a homemade, temperature-stabilized, 10.5 cm-long aluminum sample cell for spectroscopy, closed at each end by an AR-coated BK7 window.

A Labview® code was developed to acquire simultaneously, by means of a digital oscilloscope connected to a personal computer through a USB-GPIB board, the signals transmitted from the etalon, the optical resonator, and the CO_2 cell. For each laser frequency scan, a total of 5000 points were acquired with a 13-bit vertical resolution. Signal averaging (over 25 consecutive scans) allowed us to increase the signal-to-noise ratio, reducing the detection bandwidth down to about 600 Hz. So doing, the overall acquisition time per spectrum was 5 seconds.

The absorption cells were filled with pure CO_2 (with a nominal purity of 99.999%) at adjustable pressure, which was measured using a 100 Torr full-scale capacitance gauge with a 0.25% accuracy of the reading. A turbo-molecular pump was used to periodically evacuate the sample cell and create high-purity conditions.

2.1. Frequency calibration

The confocal resonator consisted of a pair of identical, high-quality, 1-inch dielectric mirrors, with a radius of curvature of 50 cm and a reflectivity of about 99.5%. The high reflectivity mirrors were held by a pair of stainless steel mounts, equipped with tilting knobs for fine alignments and tightly locked over a stainless steel base. The mounts were fitted into the two ends of a glass tube, which can be evacuated at a level of 10^{-6} Torr. The confocal cavity was aligned in an off-axis configuration, in order to excite both even and odd modes. Its free spectral range (FSR) was measured to be (149.56 ± 0.01) MHz (relative uncertainty of 6.7×10^{-5}). This value is the result of a weighted mean between the FSR values determined using two different methods. The first method, based on a broad laser frequency scan ($\sim$0.5 cm^{-1}), consisted in the observation of two CO_2 absorption lines, namely the R(8) $\nu_1 + 2\nu_2^0 + \nu_3$ and R(27) $\nu_1 + 3\nu_2^1 - \nu_2^1 + \nu_3$ transitions, whose center frequencies are accurately known [10]. The second method consists in the simultaneous detection of the absorption of both the zero- and first-order beams, as provided by the AOM, from a pair of CO_2 absorption cells kept at the same thermodynamic conditions (as it is shown in Fig. 1). Because of the frequency shift between the two beams, the center frequencies of the two line profiles, recorded along with the transmission comb from the optical cavity, are separated by a very well known quantity (equal to 80517.42 ± 0.12 kHz, as provided by an universal counter), from which the FSR can be retrieved.

During operation, typical laser scans of about 0.1 cm^{-1} were performed and frequency ruling was obtained using $\sim$20 teeth (markers) of the comb provided by the resonator. In order to take into account the non-linearity in the laser frequency tuning, introduced by the piezo-actuator controlling the external cavity length, we interpolated the frequency markers by means of a cubic spline routine. We periodically checked the accuracy of the linearization procedure by recording the transmission spectrum of the germanium etalon and by fitting each peak with an Airy function.

2.2. Absorption scale

Besides the frequency scale, we focused our attention also to the minimization of possible systematic errors in the absorption scale. The relevant sources of errors in the vertical scale are the optical zero, any error in the (assumed, modeled, or measured) spectral baseline – that is, the signal as function of frequency returned by the spectrometer in the absence of any absorption, and a possible non-linearity in the detection chain. The first issue, which strongly depends on the spectral purity of the laser source, can be completely neglected in our case as a mirror-extended laser cavity configuration was used [11]. For what concerns the baseline, rather than using background subtraction method or attempting to model them with polynomial functions, we hold the baseline flat to within 0.01% (over a 0.5 cm^{-1} scan) experimentally, using the intensity control feedback loop described above, that regulates the laser power passing through the CO_2 absorption cell. This loop had a bandwidth of 50 kHz and was able to correct for variations in laser power over the whole laser frequency scan.

In the matter of detector non-linearity, we decided to investigate this issue deeply, especially in light of the fact that it has been studied only for standard InGaAs photodiodes [12]. In fact, we tested the linearity of our detection chain, consisting of the thermoelectrically cooled extended-wavelength InGaAs photodiode (Hamamatsu Photonics, model G5853-11), its associated electronics, and the digital oscilloscope (Tektronix mod. TDS7104) used to acquire the signals, employing the optical set-up shown in the lower part of Fig. 1 (drawn using short-dashed lines). Here, a part of the main beam was sent to the photodiode Ph_4 (providing signal S_0) while another part was sent to a monitor detector ($Ph_{Monitor}$ in the figure) that provides a normalization signal S_M used to correct for possible laser output variations. Furthermore, part of the beam diffracted by the AOM impinged upon the same photodiode (Ph_4, producing

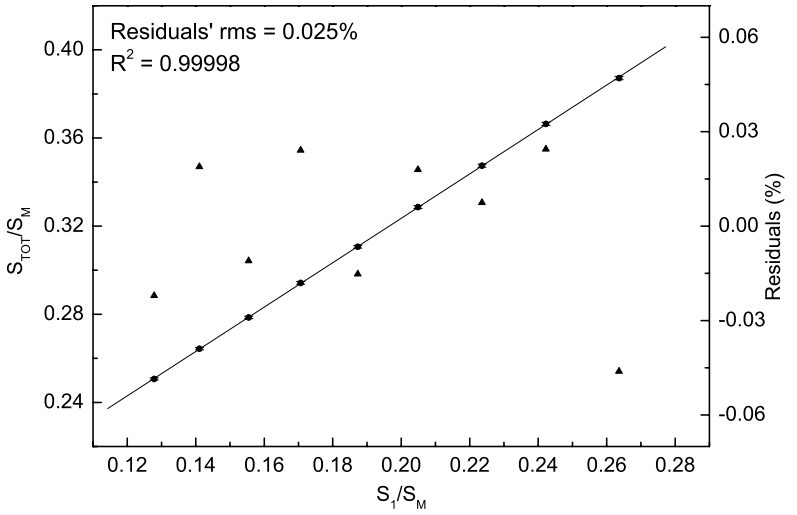

Fig. 2. Results of the linearity test of the complete detection chain, including the detector and the digital oscilloscope. We found a nearly perfect agreement with a linear correlation coefficient, R^2, of 0.99998. The acronym rms stands for root mean square value.

signal S_1). The power of the diffracted beam could be varied by changing the RF power driving the AOM, denoted with P_A. Thus, we obtained $S_1 = S_1(P_A)$. An electronic shutter in each of the two beam branches allowed for the detector to provide S_0, $S_1(P_A)$, or the signal arising from the superposition of the two beams, $S_{tot}(P_A)$. Then, in the case of a perfectly linear detector response, the following equation should be valid:

$$\frac{S_{tot}(P_A)}{S_M} = \frac{S_0}{S_M} + \frac{S_1(P_A)}{S_M} \tag{2}$$

for all P_A. Shown in Fig. 2, the results of our test indicate that the response of the complete detection chain is linear to within 0.025% for $0.25 < S_{tot}/S_M < 0.39$, simulating the situation experienced with fractional absorption between 0 and 35%. The absolute power incident on the photodiode in the linearity test (about 150 μW) was somewhat higher than that in our spectral scans (about 50 μW). To constrain the non-linearity of the detector further, we repeated our tests replacing the oscilloscope with a $6\frac{1}{2}$-digit voltmeter (Agilent, model 34401a). In this case, the scatter in the points appears reduced and the response of the detection chain was linear to within 0.016%, over the same power range. We can therefore conclude that the worst-case distortion, caused by detector non-linearity, in our experiment, could be neglected as it was always within the noise level.

2.3. Temperature stabilization

Particular attention was paid to the temperature stabilization of the absorption cell. Consisting in an aluminum block, with a cylindrical hole inside (1.7 cm diameter), it was housed in a stainless steel vacuum chamber to ensure an optimal thermal insulation. The vacuum chamber was equipped with two optical windows of the same type as those of the cell. In order to minimize heat transfer by conduction, a remote-controlled oil-free solenoid valve was installed very close to the cell, inside the chamber. The sample cell was temperature stabilized by means of four Peltier elements (two for each of the upper and lower facets of the absorption cell, each of them with a nominal power of ∼50 W), which allowed us to vary the cell body temperature between 270 and 330 K. Heat exchangers, based on water circulation, were employed for heat transport to or from the rear facets of the thermoelectric elements. Three precision platinum resistances (Pt100) were housed in the aluminum block. The first one acted as a sensor for a proportional integral derivative (PID) controller that kept the temperature uniform along the cell and constant within 40 mK, over a time interval of ∼2 h. The second and third thermometers, located at each of the two ends of the cell, were used to measure the temperature of the cell body. The PID sensor was calibrated by the Calibration Service in Italy (SIT), while the other two Pt100 sensors were calibrated at the triple point of water (TPW) and at the gallium melting point by the Istituto Nazionale di Ricerca Metrologica (INRIM). For this purpose, two special adapting probes were manufactured to properly host the Pt100 when inserted inside the well of the fixed point cells. After a series of measurements in

the TPW cell, both the Pt100 sensors showed a measurement repeatability within 0.1 mK during one month. During the calibration and when placed in the absorption cell, the platinum resistance thermometers (PRTs) were fed by a 1 mA current; the self heating effect was evaluated and the corresponding correction was applied together with the associated uncertainty. Resistance from one of this sensor was acquired, simultaneously with each laser frequency scan, by means of a $6\frac{1}{2}$-digit multimeter connected to the personal computer through the USB-GPIB board. In order to measure sensors' resistance, we used the so-called 4-wires ohms method. The short-term temperature stability (over 4 minutes, i.e. the time span of one set of spectroscopic measurements) was typically $\sim$10 mK.

3. Line shape problem and spectral analysis

Spectral line shapes are determined by the dynamics of the molecular interaction with the surrounding medium, which includes an electromagnetic field. In classical theories of pressure broadening, ignoring the internal structure of the particles and adopting the statistical mechanics formalism, the frequency response of a molecule emitting or absorbing radiation, in the presence of many other perturbing molecules, is given by the Fourier transform of the dipole correlation function $\Phi(t)$ [7,13]:

$$I(\omega) = \frac{1}{\pi} \int_0^\infty \Phi(t) \mathrm{e}^{-i\omega t}\, \mathrm{d}t \tag{3}$$

where

$$\Phi(t) = \left\langle \frac{\boldsymbol{\mu}(0) \cdot \boldsymbol{\mu}(t)}{\boldsymbol{\mu}(0)^2} \right\rangle \tag{4}$$

will allow to account for the simultaneous action of Doppler and collision broadening effects. Here, the symbol $\langle \ldots \rangle$ denotes the ensemble average, while $\boldsymbol{\mu}$ is the electric dipole moment. The line shape function will be the real part of $I(\omega)$. The ensemble average is calculated using the probability density, $f(\boldsymbol{r}, \boldsymbol{v}, t)$, that gives the probability of finding a molecule at position $\boldsymbol{r}$ and velocity $\boldsymbol{v}$ at time t. This function, describing the emitter motion, will satisfy the Boltzmann transport equation whose form depends on the physical conditions in which the spectral line is observed. For a low pressure gas, at thermodynamic equilibrium, one can make the assumption of free motion of emitters on straight-line trajectories and neglect velocity-changing collisions. Then, the kinetic equation takes the following form:

$$\frac{\partial f(\boldsymbol{r}, \boldsymbol{v}, t)}{\partial t} = -\boldsymbol{v} \cdot \boldsymbol{\nabla} f(\boldsymbol{r}, \boldsymbol{v}, t) \tag{5}$$

being $\boldsymbol{\nabla}$ the gradient operator in spatial coordinates. Assuming that at $t = 0$ the particle is in the position $\boldsymbol{r} = 0$, with a velocity distribution given by the Maxwellian function, the solution of Eq. (5) can be written in this way [7]:

$$f(\boldsymbol{r}, \boldsymbol{v}, t) = \delta^3(\boldsymbol{r} - \boldsymbol{v}t)\, f_M(\boldsymbol{v}) \tag{6}$$

where $f_M(\boldsymbol{v})$ is the Maxwellian distribution. In addition, the dipole correlation function will be given by:

$$\Phi(t) = e^{i\omega_0 t} \left\langle \exp(-i\boldsymbol{k} \cdot \boldsymbol{r}) \exp\left[-\theta(t)\right] \right\rangle \tag{7}$$

where ω_0 is the unperturbed frequency of the emitted radiation and $\boldsymbol{k}$ is the corresponding wave vector, while $\theta(t)$ is a function describing the phase shift of the emitted radiation at the time t during collisions between emitter and perturbers. Here, we have considered a linear approximation for the phase shift, namely $\theta(t) = (\Gamma + i\Delta)t$. Under the hypothesis of a negligible dependence of the collision parameters on the emitter velocity, the well known Voigt profile is obtained from Eqs. (7), (6) and (4). In fact, the complex line profile will be [7]:

$$I(\omega) = \frac{1}{\pi} \int \mathrm{d}\boldsymbol{v}\, f_M(\boldsymbol{v}) \frac{1}{\Gamma - i(\omega - \omega_0 - \Delta - \boldsymbol{k} \cdot \boldsymbol{v})} \tag{8}$$

whose real part will be the Voigt convolution, Δ and Γ being the pressure shift and width, respectively. This simple derivation clearly shows that the line shape is determined by the functions $f(\boldsymbol{r}, \boldsymbol{v}, t)$ and $\theta(t)$. In particular, the former assumes a more complicated form when the averaging effect of velocity-changing collisions cannot be neglected, leading to the occurrence of Dicke narrowing in the observed line shape. This confinement effect is usually treated

adding in Eq. (5) the term $\hat{S}_{VC} f(\boldsymbol{r}, \boldsymbol{v}, t)$, being $\hat{S}_{VC}$ the velocity-changing collision operator [14]. Under the hypothesis of soft (or weak) collisions, a diffusive character is invoked since collisions have a significant effect only collectively. In this case, the emitter motion is modeled in terms of the theory of Brownian motion. Alternatively, in the hard (or strong) collision limit, the $\hat{S}_{VC}$ operator is written in such a way to take into account that the velocity after a single collision is completely uncorrelated to the velocity prior to the collision.

In the speed-independent case, the soft collision approach yields the Galatry profile, while the hard collision limit gives a description usually referred to as Nelkin–Ghatak profile [15,16]. In both cases, velocity changes and internal state perturbations are assumed to occur in separate collisions. A generalization of the two profiles is also possible and takes into account the statistical correlation between the two processes [7]. A further line narrowing mechanism is given by the speed dependence of collisional cross sections, which may give rise to speed-dependent Voigt profile or, when acting jointly to Dicke narrowing, can lead to speed-dependent Galatry and speed-dependent Nelkin–Ghatak profiles [7].

Characterized by increasing complexity, the mentioned line shape functions give only an incomplete picture of the present (and continuously evolving) situation regarding line shape models, in the linear absorption regime. Depending on the absorbing (or emitting) molecule, gas composition and thermodynamic conditions, one of them can reproduce the molecular absorption profile very precisely. We have already demonstrated an agreement between theory and experiment at a level of a few parts over 10^5 [11]. Nevertheless, a successful interpolation does not necessarily imply high accuracy in retrieving widths and collision parameters, as it will be shown later on, in this article.

For a true calculation of a spectral line shape, one should resort to the density-matrix formalism of quantum mechanics and solve a Boltzmann-like transport/relaxation equation for the appropriate off-diagonal elements of the density matrix [14]. A similar approach has been recently reported for the simplest possible situation of an unshifted, isolated line in a diatomic gas (CO) perturbed by structure-less atoms (Ar), in order to include speed-dependent pressure broadening (with the speed-dependence obtained from quantum mechanical scattering calculations), Doppler broadening, Dicke narrowing [17]. Of course, the extension of this approach to self-colliding triatomic molecules is far from being trivial.

Hence, this situation suggests that the most reliable strategy for the implementation of Doppler broadening thermometry consists in a careful selection of the molecular target, thermodynamic conditions, absorption line and operation wavelength so that the averaging effect of velocity-changing collisions can be neglected and the line shape is well reproduced by a Voigt convolution. It is worth noting that Dicke narrowing can be ignored when the mean free path of the molecules is much larger than $\lambda/2\pi$, as it can be easily demonstrated from an uncertainty principle argument [18]. This means that the larger is the wavelength the smaller must be the gas pressure in order to satisfy this requirement.

However, any influence from Dicke narrowing or speed-dependent effect can always be verified *a posteriori* by checking the insensitivity of the retrieved Doppler width from the gas pressure, at a given temperature.

The normalized Voigt function is given by:

$$V(\nu - \nu_0) = \frac{1}{\pi^{3/2}} \sqrt{\ln 2} \frac{\Delta\nu_C}{\Delta\nu_D} \int_{-\infty}^{+\infty} \exp\left[-\frac{\ln 2(\nu' - \nu_0)^2}{\Delta\nu_D^2} \right] \frac{1}{(\nu - \nu')^2 + \Delta\nu_C^2} \, \mathrm{d}\nu' \tag{9}$$

where ν_0 is the line center frequency and $\Delta\nu_C$ the collision width (HWHM). This integral is mathematically equivalent to the real part of the complex error function, which can be evaluated only numerically. To improve the efficiency of the Voigt profile analysis of spectral lines, we used the approximation of Weideman [19]. Numerical simulations confirmed that this approximation is equal to the Voigt convolution, as tabulated in Ref. [20], to $\sim$1 part in 10^8. A MATLAB code was implemented to carry out the line shape fitting and retrieve the Doppler width in a fully automated way for any set of repeated spectral acquisitions. The non-linear least-squares fitting routine was based on a Levenberg–Marquardt algorithm. The code was tested on simulated spectra, each of them consisting in a computed Voigt profile plus a random noise. As one could expect, the relative accuracy in the retrieval of the Doppler width depends on the signal-to-noise ratio. In particular, a relative deviation between the real value and the retrieved one of 1.7×10^{-6} (mean values over 30 simulations) were found for $S/N = 1.6 \times 10^4$ (that is nearly a factor of 10 better than the present one), as it is shown in Fig. 3. The simulated absorption spectrum along with the fitting curve is reported in Fig. 4, with the residuals in its bottom part. The free parameters were the line center frequency, the homogeneous and Doppler widths, the amplitude factor and the baseline. We can therefore conclude that, as long

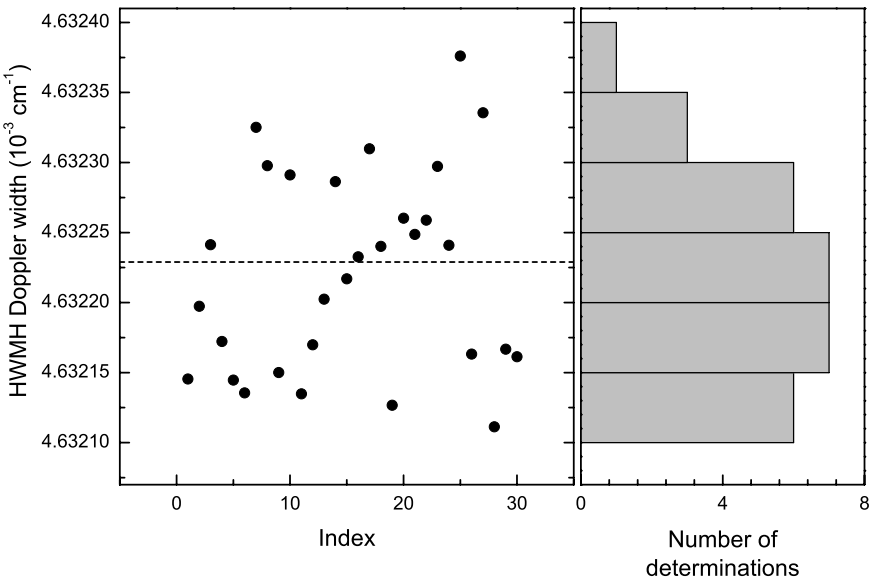

Fig. 3. Repeated determinations of the Doppler width (HWHM) from numerically simulated absorption spectra, assuming a CO_2 pressure of $\simeq$130 Pa, a temperature of 296 K, a 16-bit vertical resolution and a S/N of $\sim$16 000. The retrieved mean value is $(4.632221 \pm 0.000013) \times 10^{-3}$ cm^{-1}. The real Doppler width, indicated by a dashed line, is 4.632229×10^{-3} cm^{-1}. A histogram of the determinations is also shown.

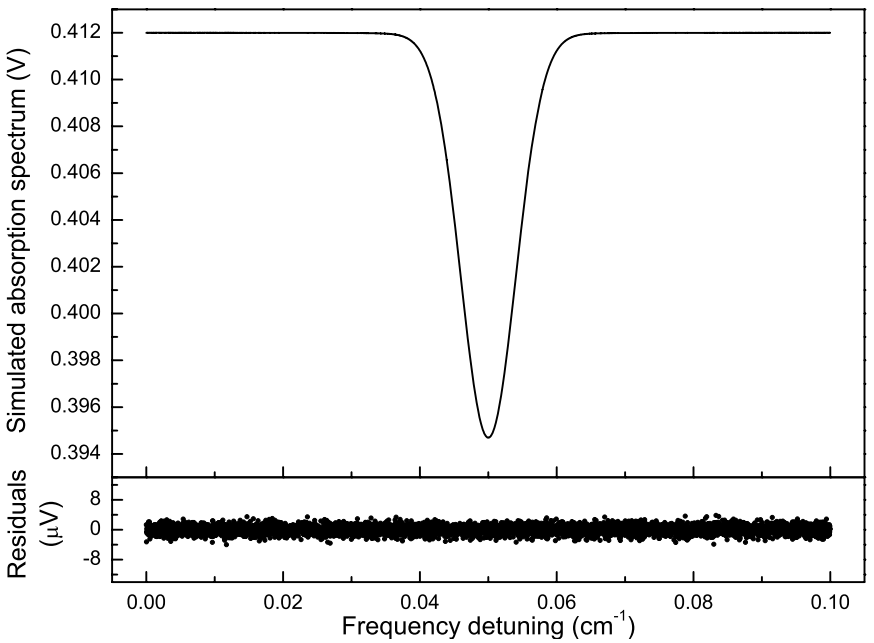

Fig. 4. Simulated absorption spectrum of the R(12) CO_2 line. The operation conditions are the same as for Fig. 3, setting the ratio between the homogeneous and inhomogeneous widths to 0.03. The absolute residuals are also shown, resulting from the application of the line fitting procedure.

as the Voigt function describes the absorption profile with undoubted physical meaning, at the required precision level, the accuracy of Doppler-broadening thermometry will not be limited by the selected computation method of the complex error function and by the fitting procedure.

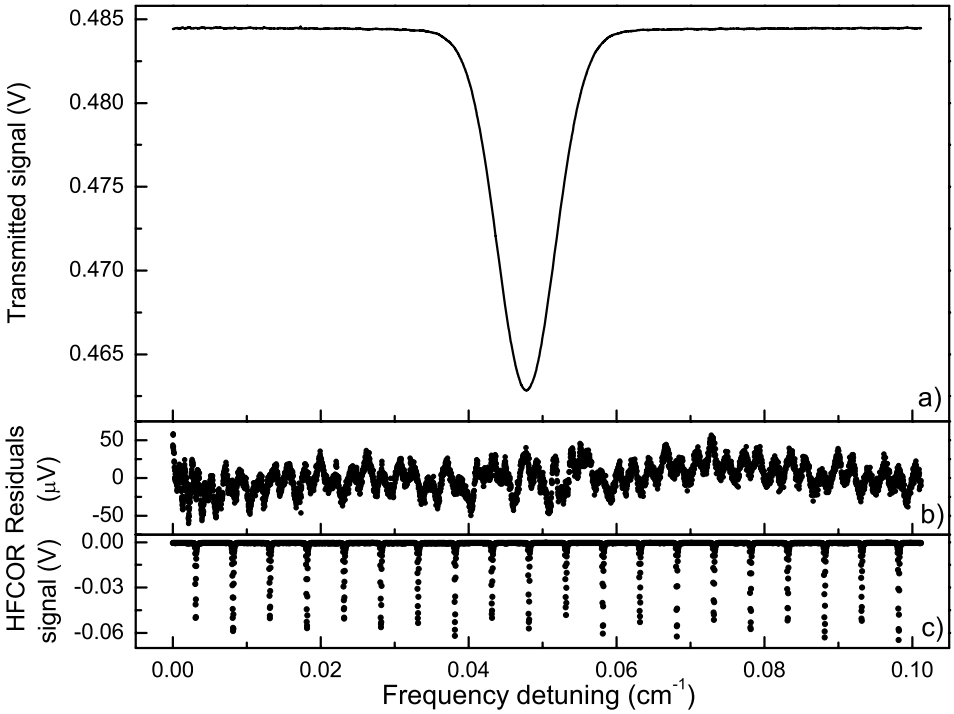

Fig. 5. Example of experimental transmission spectrum for the R(12) line at $\simeq$130 Pa and 283.09 K (a). The absolute residuals are also shown, as a result of a non-linear least-squares fit to a Voigt convolution (b). The retrieved Doppler width (HWHM) was (135.83 ± 0.03) MHz. In the bottom part of the figure (c), the transmission comb from the optical resonator is reported. The natural line width of this transition is much smaller than 1 kHz, i.e. negligible. Similarly, saturation and transit time broadening effects can be completely neglected, in our experimental conditions.

4. Results and discussion

A typical transmission spectrum is shown in Fig. 5. It corresponds to the R(12) CO_2 absorption line at a gas pressure of about 130 Pa and a temperature of 283.09 K. The measured fractional absorption was 4%, while the signal-to-noise (S/N) ratio was estimated to be about 1300:1, with an equivalent noise detection bandwidth of 600 Hz. The residuals, reported in the bottom part of the figure, clearly show that the exponential of a Voigt convolution is well capable of reproducing the spectrum through a non-linear least-squares fit. The free parameters (five, in total) were the same as for the simulations discussed above. As a result of fifty repeated determinations of the Doppler width, over a time interval of 4 minutes, we retrieved a gas temperature of (283.04 ± 0.16) K, which is in full agreement with the simultaneously recorded Pt100 temperatures (yielding a mean value of 283.09 K with a standard deviation of 10 mK). The comb of resonances, provided by the optical resonator and used for frequency calibration, is also shown.

Obviously, increasing the gas pressure, as the S/N ratio increases, an improvement in the precision level of spectroscopic determinations of the gas temperature would be expected. Nevertheless, it turns out that there is an upper limit for the gas pressure, beyond which the Voigt function becomes incapable of fitting the experimental line shape. This is clearly evidenced by the "w" structure appearing in the residuals shown in Fig. 6.

A systematic study of standard line shapes (namely, speed-dependent Voigt, Galatry, Nelkin–Ghatak, correlated Galatry, and correlated Nelkin–Ghatak profiles), including speed-dependent broadening or Dicke narrowing effects, revealed that the model best reproducing the absorption profile for self-colliding CO_2 molecules, in the pressure range between 0.7 and 4 kPa, is that of Galatry [21]. An example of a successful fit is given in the bottom part of Fig. 6. It must be noted that line fitting to the Galatry profile requires a further free parameter, as compared to the Voigt convolution, i.e. the effective frequency of velocity changing collision, β, which exhibits a significant correlation with the homogeneous and Doppler widths. The β parameter resulted to be unrealistically large, as compared to the prediction based on the mass diffusion coefficient. As a consequence, the Doppler width resulted to be overestimated when using the Galatry profile. In fact, line fitting to the Galatry function, performed on fifty repeated spectral ac-

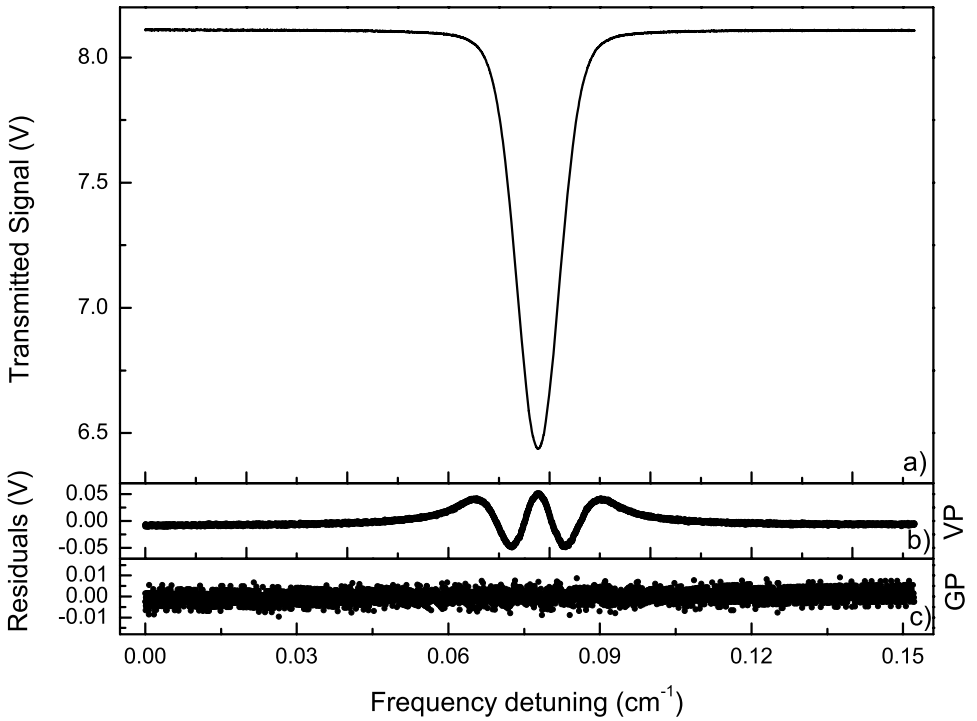

Fig. 6. Transmission spectrum for the R(12) line at a pressure of ≃650 Pa and a temperature of 280.32 K. In the lower part of the figure, the absolute residuals are shown, as a result of a non-linear least-squares fit to the Voigt profile (VP) and to the Galatry profile (GP). The Doppler width (HWHM) of the VP function was set to the expected value, i.e. $\Delta\nu_D = 0.00451\ \mathrm{cm}^{-1}$.

quisitions, similar to that of Fig. 6, yielded a gas temperature of (288.1 ± 0.5) K, which does not agree with the real one (280.32 ± 0.01) K and exhibits a larger statistical uncertainty. On the other hand, we have found good indications that the collisional broadening coefficients are not significantly affected by the model's difficulties in treating the narrowing, as discussed elsewhere [21].

Therefore, we can conclude that spectroscopic measurements of the gas temperature has to be performed in the low pressure regime (below ∼200 Pa, so that the mean-free-path of the molecules is at least a factor of 10 larger that the wavelength), as none of the tested models is completely appropriate to describe the physical situation of the CO_2–CO_2 system. By the way, this is a first valid reason for moving to another physical situation, such as that of self-colliding H_2O molecules. A severe test of the operation of the spectrometer as a primary thermometer was performed, varying the gas temperature, but always setting the CO_2 pressure to values around 100 Pa. With very few exceptions, a good agreement was found between the spectroscopic and the Pt100 temperatures, typical deviations being much smaller than 1 K.

4.1. Spectroscopic determination of k_B

We now move to the spectroscopic determination of the Boltzmann constant. We performed Doppler width determinations for different values of the gas temperature, in the range between the triple point of water and the gallium melting point. This approach was adopted at the purpose of converting possible temperature dependent systematic errors into statistical ones. A linear fit of the $\Delta\nu_D^2$ data versus T provided the spectroscopic value for the Boltzmann constant, namely $k_B = 1.38058(13) \times 10^{-23}\ \mathrm{J\,K^{-1}}$, the quoted uncertainty being the statistical error on the slope of the weighted best-fit line [8]. The molecular mass, appearing in Eq. (1), was calculated from the relative atomic masses of ^{16}O and ^{12}C, the molar mass constant and the Avogadro number [22]. This value resulted from the analysis of about 1500 spectra, acquired over five consecutive weeks and involving twelve different values of the temperature. In order to quantify the accuracy level of this determination, we performed an uncertainty budget, which is summarized in Table 1. We considered all the possible sources of both random and systematic uncertainties. The first entry of Table 1

Table 1
Uncertainty budget (in terms of relative errors) for the spectroscopic determination of k_B.

Source	Random errors	Systematic errors
Slope of the best fit line	9×10^{-5}	
Frequency calibration		1.3×10^{-4}
Frequency scale non-linearity		Negligible
Cavity alignment		$\leqslant 2 \times 10^{-7}$
Cavity temperature		$\leqslant 6 \times 10^{-5}$
Instrumental line width		$\leqslant 6 \times 10^{-6}$

is the statistical error on the slope of the best-fit line. We believe that it should include also those systematic errors that are characterized by a non-monotonous temperature dependence. This is the case of spurious etalon effects due to the cell's windows and clearly visible in Fig. 5, whose effect on the temperature retrieval can be randomized (in its entity and sign) by varying the cell's temperature.

The main source of error is surely the frequency calibration procedure, based upon on the high finesse optical cavity. The relative uncertainty of the cavity FSR, multiplied by a factor 2, contributes to the overall uncertainty on k_B with a relative quantity of 1.3×10^{-4}.

In order to better quantify the accuracy in the horizontal (i.e. frequency) scale, we also considered the influence of temperature variations and of changes in the confocal cavity alignment on the FSR splitting frequency. The temperature inside the laboratory was stabilized within ± 2 K. This could lead to a maximum relative variation of the cavity FSR of 2.8×10^{-5}. However, as a result of our strategy for determining k_B, this uncertainty should be randomized and, therefore, its influence should be already included in the statistical error of k_B. For what concerns the alignment, we can calculate that in the worst case (namely, the beam at the edge of the mirror with the maximum inclination) the FSR differs from the expected value by a relative amount of 1.0×10^{-7} (see for example [23]).

A further aspect deserving a discussion is a possible residual non-linearity in the frequency scale. In this respect, we can not exclude subtle wobbles between frequency markers, being the calibration and linearization procedure based upon a cubic spline fit. We have sporadically seen spikes in the residuals' structure that could be ascribed to those wobbles. They surely contribute to the overall random error, since they should act as a source of fluctuation in repeated determinations of the Doppler width at a given gas temperature. Apart from these wobbles, no significant deviations from linearity were evidenced. An a posteriori justification to this statement is provided by the fact that no asymmetry and/or distortion can be found in the absorption spectra, at the present noise level, as clearly evidenced by the residuals at any pressure (see Figs. 5 and 6).

As for the instrumental line width, in principle it should be convolved into the spectrum. We tested its influence by comparing fits of simulated spectra with and without accounting for the laser emission width. We found that for a Lorenztian laser profile (which is expected in the case of a mirror-extended DFB diode laser, as reported in [24]), with a 1-MHz width, the fractional error induced in the retrieved Doppler width, under our experimental conditions, was below 3×10^{-6}.

Temperature fluctuations in the short-term, i.e. the time interval of $\sim$4 minutes that is covered by fifty repeated spectral acquisitions, were of the order of 10–15 mK (one standard deviation), which is typically a factor of 10 smaller than the fluctuation of repeated spectroscopic determinations of the temperature itself. Regarding the temperature uniformity of the gas cell, we have provided a very conservative estimate (40 mK), obtained at the lowest temperature. Nonetheless, we think that systematic deviations arising from a small temperature non-uniformity could be neglected. In fact, the transmitted laser beam should carry information on the spatially averaged value of the gas temperature, along the cell axis (this is not exact in principle, but is true to a very good approximation in our case). Variations in the transverse direction should be neglected because of the small size of the laser beam ($\sim$5 mm), the small power ($\sim$50 μW) and the small fractional absorption ($\sim$4%). However, the temperature non-uniformity, as well as its possible effect on the retrieved Doppler widths, are likely to vary with the cell's temperature. As for the spurious etalon effects, we believe that these possible systematic deviations are converted into random errors, which should be already included in the statistical uncertainty on k_B. Similarly, the uncertainty on the cell's temperatures is already included in that of the slope (reported in the first line of Table 1). Taking into account all the sources of errors, the 1-σ uncertainty on k_B increases up to 22×10^{-28} J K^{-1}, which translates into a relative uncertainty of 1.6×10^{-4}. Our

value agrees with the CODATA one, as well as with the spectroscopic determination recently performed by Daussy et al. on $^{14}NH_3$ in the mid-infrared [9].

4.2. Towards an improved determination of k_B

We are presently going through the implementation of a new spectroscopic apparatus showing high-resolution and excellent signal-to-noise ratio, while keeping any source of line distortion at the lowest level. Very briefly, the water spectrometer is based on a reference diode laser (master laser), frequency stabilized against the saturated absorption of a vibration-rotation line of $H_2{}^{17}O$ at 1384.5919 nm, a tunable diode laser (slave laser) phase locked to the reference one, and an isothermal water vapour cell referenced to the temperature of the triple point of water. The slave laser probes a vibration-rotation line of $H_2{}^{18}O$ at 1384.6008 nm. The two laser sources, of the InGaAsP (Fabry–Pérot) type, are mounted in extended cavity configuration. Water vapour represents an optimum choice as a molecular target for a number of reasons. First of all, collisional effects in its vibration-rotation spectrum have been the subject of many experimental and theoretical efforts, in the last twenty years. The H_2O molecule exhibits strong vibro-rotational lines around 1.4 μm. These absorption features belong to the $\nu_1 + \nu_3$ and $2\nu_1$ vibrational bands and have been already investigated by our group, in recent years [25,26]. We observe that hyperfine structure effects can be completely neglected as, at the first order, magnetic dipole and electric quadrupole effects do not occur. In fact, the electronic ground state of the H_2O molecule is a singlet sigma state, while the nuclear spin of H atoms is $\frac{1}{2}$.

A detailed description of the new spectrometer would be beyond the aims of the present article. Therefore, we limit this section to highlighting the most important features that should allow us to approach the target accuracy of 10^{-6}.

In Section 4.1, we have seen that the main source of error is given by the frequency calibration procedure. This limitation will be completely overcome by the use of the phase locking technique, which gives the possibility to perform broad scans of the slave laser around an arbitrary center frequency with an accuracy at a level of 10 kHz, determined by the emission line width of the master oscillator. As for the temperature of the sample cell, the newly developed (and already tested) system ensures a constant and homogeneous gas temperature within 1 mK. Similarly, no limitation is expected by the linearity feature of the photodetector. In fact, by shifting the operation wavelength down to 1.4 μm, we will be able to exploit the excellent performances of standard InGaAs photodiode, whose linearity was reported to be 0.08% for the large photocurrent range between 10^{-7} and 10^{-4} A [12].

Further advantages arising from a reduced wavelength of operation are, obviously, the larger Doppler width and the shorter length parameter ($\lambda/2\pi$), relevant for the Dicke narrowing effect. In other words, the requirement on the mean free path of the molecules that must be satisfied in order to neglect velocity changing collisions, should be more relaxed as compared to the 2-μm experiment. Simulations similar to those discussed in Section 3, performed on the $H_2{}^{18}O$ line at 1384.6008 nm, for a signal-to-noise ratio of 2×10^4, have shown that an accuracy level of $\sim 10^{-6}$ can be achieved in the retrieval of the Doppler width by using a Voigt convolution. Of course, once we will be able to retrieve the Doppler width with such a small uncertainty, it will be necessary to check its constancy as a function of the gas pressure. If a dependence will be found, we plan to exploit the recent progress in the reconstruction of the spectral line shape of the H_2O–H_2O system, accounting for both Dicke narrowing and speed dependence of the broadening and shifting parameters [27].

5. Conclusions

The Doppler broadening effect, which is usually eliminated in any experiment of time and frequency metrology, can be regarded as a gift of nature for the purpose of measuring the thermodynamic temperature of any gaseous sample. We have discussed a proof-of-principle experiment in which Doppler broadening thermometry has been implemented and used for the spectroscopic determination of the Boltzmann constant, exploiting the relatively strong absorption spectrum of CO_2 molecules in the wavelength window around 2 μm. The experimental strategy for retrieving k_B consisted in measuring the Doppler width of a given vibration-rotation line at a constant pressure (of the order of 100 Pa) as a function of the temperature, accurately determined by means of precision platinum resistance thermometers. At the present level of accuracy, we did not observe any influence of Dicke narrowing or speed-dependent effects. In other words, the Voigt profile resulted to be physically meaningful in reproducing the spectral line shape. A detailed study on the sources of uncertainties, of both random and systematic type, allowed us to identify in the frequency

calibration procedure the main source of error. Then, we found that there exist huge margins of improvements, which are being already pursued in the second generation experiment on the near-infrared spectrum of the H_2O molecule.

Acknowledgements

This work was partially funded by the Italian Ministry for University and Research, under the framework program PRIN 2006. Three authors (A.C., G.C. and L.G.) also acknowledge the support provided by the Regione Campania under the program Legge n. 5/2005.

References

[1] G.J. Padilla-Viquez, J. Koelliker-Delgado, O. Werhahn, K. Jousten, D. Schiel, IEEE Trans. Instr. Meas. 56 (2007) 529–532.
[2] Ch.J. Bordé, Metrologia 39 (2002) 435–463.
[3] Ch.J. Bordé, Phil. Trans. Roy. Soc. A 363 (2005) 2177–2201.
[4] M.P. Arroyo, R.K. Hanson, Appl. Opt. 32 (1993) 6104–6116.
[5] M.P. Arroyo, T.P. Birbeck, D.S. Baer, R.K. Hanson, Opt. Lett. 19 (1994) 1091–1093.
[6] R. Wehr, E. McKernan, A. Victu, R. Ciurylo, J.R. Drummond, Appl. Opt. 42 (2003) 6595–6604.
[7] R. Ciurylo, Phys. Rev. A 58 (1998) 1029–1039.
[8] G. Casa, A. Castrillo, G. Galzerano, R. Wehr, A. Merlone, D. Di Serafino, P. Laporta, L. Gianfrani, Phys. Rev. Lett. 100 (2008) 200801.
[9] C. Daussy, M. Guinet, A. Amy-Klein, K. Djerroud, Y. Hermier, S. Briaudeau, Ch.J. Bordé, C. Chardonnet, Phys. Rev. Lett. 98 (2008) 250801.
[10] C. Miller, L. Brown, J. Mol. Spectrosc. 228 (2004) 329–354.
[11] G. Casa, D.A. Parretta, A. Castrillo, R. Wehr, L. Gianfrani, J. Chem. Phys. 127 (2007) 084311.
[12] H.W. Yoon, J.J. Butler, T.C. Larason, G.P. Eppeldauer, Metrologia 40 (2003) S154–S158.
[13] S.G. Rautian, I.I. Sobel'man, Sov. Phys. Uspekhi 9 (1967) 701–716.
[14] D.A. Shapiro, R. Ciurylo, J.R. Drummond, A.D. May, Phys. Rev. A 65 (2002) 12501.
[15] L. Galatry, Phys. Rev. 122 (1961) 1218–1223.
[16] M. Nelkin, A. Ghatak, Phys. Rev. 135 (1964) A4–A9.
[17] R. Wehr, R. Ciurylo, A. Vitcu, F. Thibault, J.R. Drummond, A.D. May, J. Mol. Spec. 235 (2006) 54–68.
[18] P.L. Varghese, R.K. Hanson, Appl. Opt. 23 (1984) 2376–2385.
[19] J.A.C. Weideman, SIAM (Soc. Ind. Appl. Math.) J. Numer. Anal. 31 (1994) 1497–1501.
[20] M. Abramowitz, A. Stegun, Handbook of Mathematical Functions, Dover, New York, 1972.
[21] G. Casa, R. Wehr, A. Castrillo, E. Fasci, L. Gianfrani, J. Chem. Phys. 130 (2009) 184306.
[22] P.J. Mohr, B.N. Taylor, Rev. Mod. Phys. 77 (2005) 1–105.
[23] W. Demtroeder, Laser Spectroscopy, second ed., Springer-Verlag, Berlin, 1996.
[24] C.K. Laue, R. Knappe, K.J. Boller, R. Wallenstein, Appl. Opt. 40 (2001) 3051–3059.
[25] G. Gagliardi, G. Rusciano, L. Gianfrani, Appl. Phys. B 70 (2000) 883–888.
[26] L. Moretti, A. Sasso, L. Gianfrani, R. Ciurylo, J. Mol. Spec. 205 (2001) 20–27.
[27] H. Trana, D. Bermejo, J.-L. Domenech, P. Joubert, R.R. Gamache, J.-M. Hartmann, J. Quant. Spectrosc. Radiat. Transfer 108 (2007) 126–145.